The kinetic energy dependence of association reactions. A new thermokinetic method for large systems

Hideya Koizumi and P. B. Armentrout[a)]
Department of Chemistry, University of Utah, Salt Lake City, Utah 84112

(Received 5 June 2003; accepted 29 September 2003)

The reactions of bare alkali metal ions ($M^+ = Li^+$, Na^+, or K^+) with dimethoxyethane ($CH_3OCH_2CH_2OCH_3$, DXE) are studied using guided ion beam tandem mass spectrometry. The bimolecular reaction forms an associative M^+(DXE) complex that is long-lived and dissociates back to the reactants. The kinetic energy dependences of the cross sections for formation of the complexes are interpreted with several different models (including rigorous phase space theory) that assume that the complex lifetimes are limited by dissociation over a loose, orbiting transition state. After accounting for the effects of multiple ion–molecule collisions, internal energy of the reactant ions, Doppler broadening, and dissociation lifetimes, the analyses yield 0 K bond energies as the only adjustable parameter. These values are compared with bond energies obtained from previous collision-induced dissociation (CID) studies of the M^+(DXE) complexes and found to be self-consistent for all models studied. Association and CID form the same energized M^+(DXE) complex in two distinct ways, such that a comparison of these results allows an assessment of the models used to interpret CID thresholds and test the limits of statistical theories such as RRKM and phase space theory. © *2003 American Institute of Physics.* [DOI: 10.1063/1.1627758]

I. INTRODUCTION

Previously, Dunbar and co-workers have studied radiative association and associative equilibria using Fourier-transform ion cyclotron resonance (FT-ICR) mass spectrometry.[1,2] The analysis of the association kinetics provides a quantitative determination of clustering and complexation bond strengths. One potential criticism of this approach is that often only one data point is available for the analysis such that the approach relies exclusively on reproducing a single absolute association rate.

Guided ion beam mass spectrometry is a powerful means of studying ion chemistry in the gas phase because it provides the kinetic energy dependence of reaction cross sections under single collision conditions. In many experiments, collision-induced dissociation (CID) is used to obtain thermodynamic information by measuring the energy onset for a process such as reaction (1), where M is a metal atom, L is a ligand, and Rg is a rare gas, Xe, in most cases in our laboratories.

$$M^+L_x + Rg \rightarrow M^+L_{x-1} + L + Rg. \quad (1)$$

CID provides a direct measurement of the bond dissociation energy, although a detailed analysis of these experimental data is necessary to extract high quality quantitative thermodynamic information.[3,4] Our analysis typically includes an examination of the effect of neutral pressure, internal energy of the reactants, motion of the neutral reagent, ion beam energy spread, collisional energy transfer efficiencies, and lifetime effects (kinetic shifts). Methods for such a detailed analysis have been introduced and tested for many chemical reactions,[3,5] and have enabled the study of increasingly large complexes.[6–13] As the systems increase in complexity, the precision of the thermochemistry becomes more and more reliant on the models used for analysis, in particular because of lifetime effects. Lifetime effects in CID studies have been challenging to treat accurately[3–5] because the energized molecule is generated with a broad distribution of energies, ranging essentially from zero to the collision energy plus the internal energy of the reactant complex (for initial collisions at large and zero impact parameter, respectively). Further, the angular momentum distribution of the collisionally energized molecule is poorly characterized.

In this paper, we investigate the reactions of alkali metal ions (Li^+,Na^+,K^+) with dimethoxyethane ($CH_3OCH_2CH_2OCH_3$, DXE) molecules as a function of kinetic energy using guided ion beam tandem mass spectrometry. These systems react by association to form M^+(DXE) complexes with well-known internal energy, essentially the collision energy plus the internal energy of the DXE reactant plus the M^+–DXE bond energy, D(M^+–DXE). Both the collision energy and internal energy have known distributions. The M^+(DXE) association complex formed in this way may then dissociate back to the reactant on a time scale that can be modeled using statistical unimolecular decay theory once it is assumed that dissociation is limited by a loose, orbiting transition state (an assumption that can be tested by the success or failure of the approaches described below). The relationship between association and CID reactions is illustrated in Fig. 1, which shows a schematic potential energy surface for the M^+(DXE) system. An important facet of the present work compared to the CID studies is that the bimolecular reaction of M^+ with DXE forms an energized M^+(DXE) complex with a well-defined internal energy distribution and a broad but known angular momentum

a)Electronic mail: armentrout@chem.utah.edu

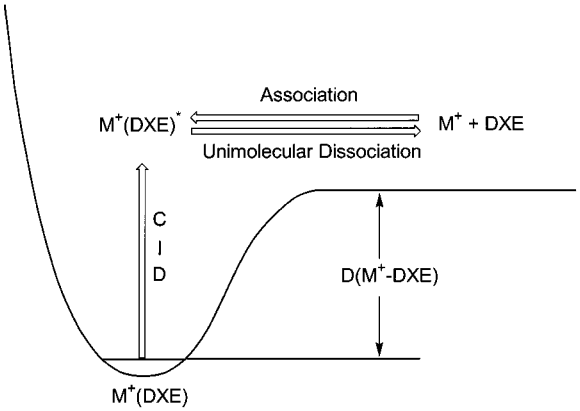

FIG. 1. Potential energy surface for association and collision-induced dissociation (CID) reactions. Two distinct way of forming the energized $M^+(DXE)^*$ molecule are shown. For CID, $M^+(DXE)^*$ is prepared at room temperature and collisionally excited with a broad internal energy distribution and unknown angular momentum distribution. In the association reaction, $M^+(DXE)^*$ complexes are formed with well-characterized distributions by reacting the bare metal ion with the DXE neutral gas at room temperature.

distribution. By comparing these results to those obtained from an analysis of CID data on the same systems,[7–9] the present study provides an opportunity to examine assumptions regarding the use of statistical theory to describe kinetic shifts observed in CID studies. In addition, we find that this work provides insight into the application of unimolecular theory, such as Rice–Ramsperger–Kassel–Marcus (RRKM)[14] and phase space theory[15–21] (PST) to rapidly rotating complexes.

II. EXPERIMENTAL METHODS

The reactions of alkali metal ions ($M^+ = Li^+, Na^+, K^+$) with DXE are examined using a guided ion beam tandem mass spectrometer described previously.[22–24] Alkali metal ions are generated in a continuous dc discharge[25] by argon ion sputtering of a cathode made from tantalum with a cavity containing the alkali metal sample. Typical operating conditions of the dc discharge are 1.6–2.0 kV and 20–30 mA in a flow of roughly 10% argon in helium. Ions then travel down a 1 m long flow tube operating at a pressure of 0.5–0.7 Torr with a helium flow rate of 5000–9000 standard cm^3/min (sccm). The flow conditions used in this ion source provide approximately 10^5 collisions between an ion and the buffer gas. Because the formation of excited states is very energetic, all alkali metal ions are produced in their ground electronic state (^1S).

The alkali metal ions are extracted from the source, accelerated, and focused into a magnetic sector momentum analyzer for a mass analysis. The mass-selected ions are slowed to a desired kinetic energy and focused into a rf octopole ion guide.[26] The guide passes through a static gas cell containing the DXE gas.[22] After exiting the gas cell, product, and remaining reactant ions drift to the end of the octopole, where they are extracted and focused into a quadrupole mass filter for mass analysis. A secondary electron scintillation ion counter detects the mass-analyzed reactant and product ions. These signals are converted to absolute reaction cross sections, as described previously.[22] Absolute uncertainties in these cross sections are estimated to be ±20%.

Sharp features in observed cross sections are broadened by thermal motion of the DXE gas and the distribution of ion energies. The distribution and absolute zero of the ion kinetic energies are measured using the octopole as a retarding potential analyzer.[22] The experimental cross section is determined by the relation

$$I_R = (I_R + I_c)\exp(-\sigma n l), \tag{2}$$

where n, l, I_R, and I_c are the gas density, effective pathlength, and the measured intensities of the reactant ion and long-lived association complex, respectively.[22] The uncertainty in the absolute energy scale is ±0.05 eV (lab). Our beam distributions have a full width at half-maximum (fwhm) of about 0.3–0.9 eV (lab). A larger fwhm (0.9 eV) is observed for Li^+ as a consequence of lithium's light mass. Kinetic energies in the laboratory frame are converted to ion energies in the center-of-mass (CM) flame by $E(\mathrm{CM}) = E(\mathrm{lab})\, m/(M+m)$, where M and m are ion and neutral reactant masses, respectively. At very low energies, the conversion includes a correction for truncation of the ion beam energy distribution.[22] All energies cited are in the CM frame, except as noted.

III. RESULTS

A. Experimental cross sections and their pressure dependence

Experimental cross sections taken at several different pressures for the reaction of all three alkali metal ions with DXE are shown in Fig. 2. In all reactions studied here, the only product observed is the association complex, as indicated in reaction (3),

$$M^+ + DXE \rightarrow M^+(DXE), \tag{3}$$

where M^+ is the alkali metal ion. In all three systems, the association complexes exhibit cross sections that decline with increasing energy, consistent with exothermic barrierless processes. The largest cross section magnitude (~100 $Å^2$ at 0.1 eV in the CM frame) is observed for $Li^+(DXE)$ followed by $Na^+(DXE)$ (~50 $Å^2$) and the smallest is $K^+(DXE)$ (~2 $Å^2$). In all cases, the association cross sections lie below the Langevin–Gioumousis–Stevenson (LGS) collisional capture cross sections,[27]

$$\sigma_{\mathrm{LGS}}(E) = \pi(2\alpha e^2/4\pi\varepsilon_0 E)^{1/2}, \tag{4}$$

where E is the collision energy, α is the polarizability volume of DXE (9.94 $Å^3$),[28] e is the electron charge, and ε_0 is the permittivity of vacuum. The LGS equation is appropriate for the present experimental cases because the ground state conformation of DXE is *trans, trans, trans*,[7] which has no permanent dipole. (The low-lying *trans, gauche, trans* conformer does have a dipole, estimated to be 2.0 D. The possible consequences of this are considered in our analysis below). In all cases, the association complex cross sections

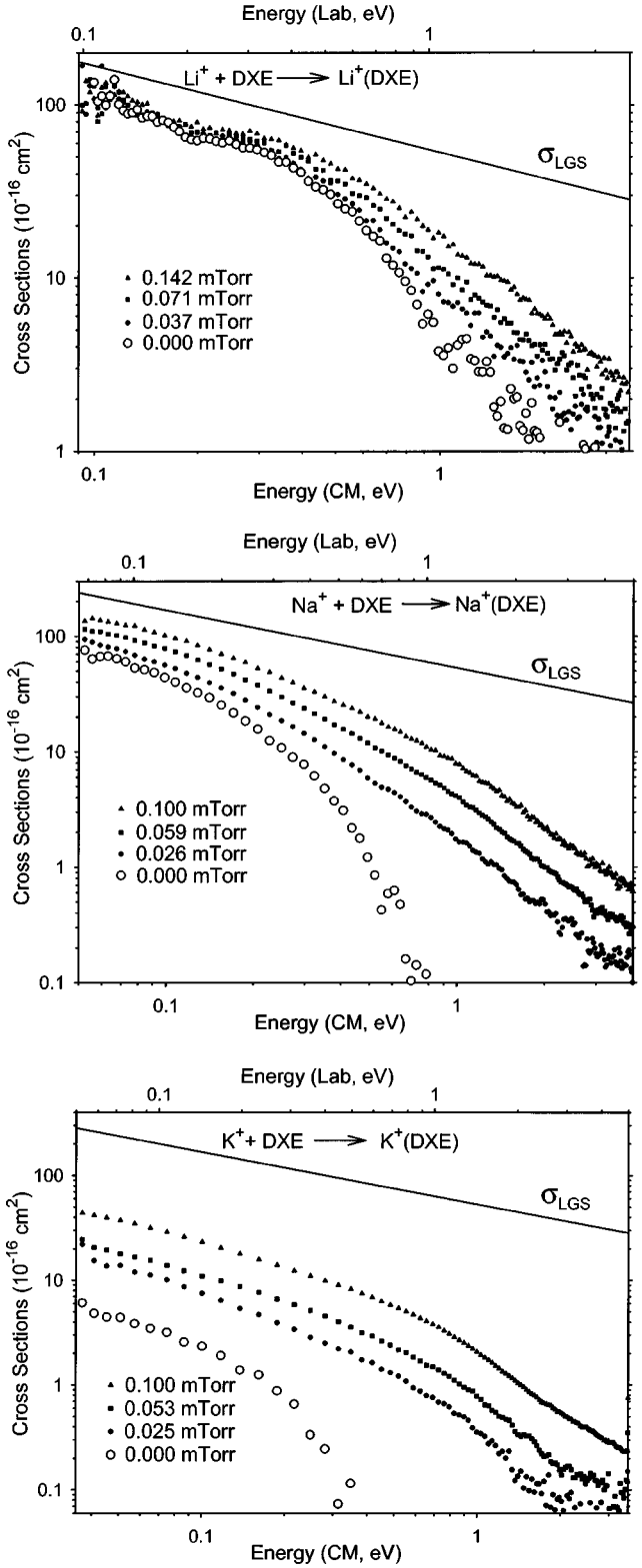

FIG. 2. Cross sections for the association reactions of alkali metal ions (Li^+,Na^+,K^+) with DXE as a function of kinetic energy in the center-of-mass frame (lower x axis) and laboratory frame (upper x axis). Small symbols indicate cross sections obtained at different DXE pressures. Open circles show the zero pressure extrapolated cross section. The solid line shows the LGS cross section, Eq. (4).

decline more rapidly than the LGS collision capture cross section at high energies because of the reformation of reactants, $M^+ + DXE$, a dark channel that cannot be explicitly monitored.

In all cases, the cross sections show a clear pressure dependence, which indicates the occurrence of collisional stabilization of $M^+(DXE)$ by secondary collisions. The effect of secondary collisions can be eliminated completely by linear extrapolation of the cross section data to zero reactant pressure.[22] Our cross sections show a clear linear dependence on pressure in all three reactions at all energies except for the $Li^+(DXE)$ cross sections at very low energies where the cross sections vary little with pressure. This lack of pressure dependence suggests that the formation of $Li^+(DXE)$ complexes is already saturated (i.e., near the LGS collision limit) at these energies. We believe that the $Li^+(DXE)$ cross section lies below the LGS cross section because of the light mass of lithium combined with the thermal motion of the neutral. At low ion kinetic energies, this combination can lead to complexes that are backscattered in the laboratory frame and not collected. Thus, at these low energies, the $Li^+(DXE)$ cross section is anomalously low. As the momentum of the ion increases (either by increasing the ion energy or its mass), such backscattered ions eventually disappear. Thus, the more massive Na^+ and K^+ systems clearly show a pressure dependence even at low energies, indicating that there is no backscattering occurring in these systems. All cross sections discussed below correspond to the zero pressure cross sections.

B. Thermochemical analysis of the associative reaction

We have modeled these association complex cross sections in three different ways. In all models, it is assumed that dissociation occurs along an ion-induced dipole potential and that the calculation of the unimolecular decay rate constant treats the transition state in the phase space limit (PSL), using equations originally developed to describe the dissociation in CID.[3] The three models differ only in how the angular momentum of the complexes is treated. Model 1 makes a similar assumption to that used to model CID reactions, namely it assumes a statistical distribution of the angular momentum in the inactive two-dimensional (2-D) rotor of the complex (external rotation around the axes perpendicular to the reaction coordinate), a common assumption for unimolecular decay theory.[29] However, this assumption fails to conserve angular momentum. In order to approximately correct this problem, model 2, which conserves the orbital angular momentum explicitly, was developed. No coupling between orbital and rotational angular momentum of the reactants or products is considered in this model and the rotational energy of the products is considered to be statistically distributed. The third model is phase space theory (PST), the rigorous statistical theory that conserves angular momentum and allows coupling between rotational and orbital motion. This should be the ideal way to calculate the rate constant for the orbiting transition state. However, the PST approach sometimes breaks down when the complex formation involves the formation of several bonds, molecular rearrangements, steric interactions, situations in which hard sphere interactions are important within the range of the phase space transition state, or when the transition state switches from long-range to short-range interactions as a

function of energy.[1] Because this study provides good opportunities to test the limits of such statistical models, these models are developed more thoroughly in this section.

It is also worth noting that we investigated several alterations of these models that were excluded from the final analysis because the alterations do not change the resulting BDEs significantly. First, we considered whether to include the centrifugal distortion in the rotational energy defined using Eq. (5),

$$F(J)=hcBJ(J+1)+hcDJ^2(J+1)^2, \quad (5)$$

where h, c, B, and J are Planck's constant, the speed of light in vacuum, the rotational constant of the complex, and the rotational angular momentum quantum number. D is given as $D=4B^3/\nu^2$, where ν is the vibrational frequency of the reaction coordinate. However, the perturbation on the rotational energy is less than 5% in all systems at any energies where the observed cross sections are nonzero. Therefore, this effect is not considered further.

Second, the radiative relaxation of the association complexes was investigated for all reactions studied here because the emission of infrared photons can stabilize the complexes. The radiative rate constants[30] at thermal energies were calculated using the VARIFLEX code[31] and found to be less than 60 s^{-1} for all three systems studied. For the time scale of the present experiments (10^{-3} s; see below), less than 6% of the complexes relax by radiation. In addition, the radiative rate constant increases slowly compared to the unimolecular rate constant as the internal energy of the complexes. Therefore, radiative relaxation does not play a significant role at any energy for all systems studied here.

Before a comparison with the data, all model cross sections are convoluted with the translational energy distributions of both reactants, as detailed elsewhere. Briefly, Lifshitz *et al.*[32] adopted the exact treatment of the Doppler broadening (neutral reactant motion) developed by Chantry,[33] in conjunction with an exact treatment of the incident ion beam distribution. Here, we use the double integral form developed by Lifshitz *et al.*[32] at very low energies because of its superior numerical accuracy over the single integral form.[22]

1. Statistically distributed inactive 2-D rotor

The first model considered is explored because it directly parallels the treatment of kinetic shifts used in modeling collision-induced dissociation processes.[3] As such, the theoretical machinery and computer code necessary was already available in our laboratory. As will be seen, model 1 provides an interesting counterpoint to the other models developed later in the manuscript. In model 1, the probability of forming a transient $M^+(DXE)$ complex is assumed to equal the theoretical LGS collision capture cross section.[27] Once the $M^+(DXE)$ complex is formed, it can undergo unimolecular decomposition back to the reactant. Thus, the cross section for formation of the $M^+(DXE)$ association complex is given by

$$\sigma_{ass}(E)=\sigma_{LGS}\sum_i g_i\int_0^{J_{max}} f(J)\exp[-k(E^*,J)\tau]dJ, \quad (6)$$

where $k(E^*,J)$ is the energy and angular momentum-dependent rate constant for unimolecular dissociation back to reactant, E^* is the available energy defined as $E^*=E+E_i+E_0$, $E_0=D(M^+-DXE)$, τ is the flight time, J_{max} is the maximum rotational quantum number as limited by the energy available,[3] and $f(J)$ is the normalized statistical distribution of the angular momentum quantum number J, described below.[3,34] The sum is over the rovibrational states of the reactant ion, having energies E_i and populations g_i (where $\Sigma g_i=1$). The Beyer–Swinehart algorithm is used to calculate the distribution of internal states of the DXE reactant at 305 K, the temperature of the gas in the reaction cell.[35–38] The flight time used can be either the energy-dependent flight time described elsewhere[39] or an average fixed flight time (1×10^{-3} s for the systems investigated here). The average flight time is larger than the value usually cited for our double octopole apparatus[24] (5×10^{-4} s) because association reactions occur primarily at lower kinetic energies than typical CID systems. Indeed, in unpublished work on the related Cu^+ + DXE association reactions, we have directly measured a time of flight of about 1 ms for the $Cu^+(DXE)$ complex.

The unimolecular rate constant $k(E^*,J)$ in Eq. (6) is defined in the usual manner by RRKM theory,[14]

$$k(E^*,J)=sN^\dagger[E^*-E_R^\dagger(J)-E_0]/h\rho[E^*-E_R(J)], \quad (7)$$

where s is the reaction degeneracy (in the present systems, unity), $N^\dagger[E^*-E_R^\dagger(J)-E_0]$ is the sum of rovibrational states of the transition state (TS), and $\rho[E^*-E_R(J)]$ is the density of states of the energized molecule (EM). $E_R^\dagger(J)$ and $E_R(J)$ are the rotational energies of the TS and EM, respectively, for the inactive 2-D external rotation. The detailed calculation of the rate constant is accomplished using equations developed by Rodgers *et al.*[3] Briefly, the TS for dissociation is modeled as loosely interacting products such that both fragments are free to rotate, i.e., a phase space limit (PSL) or, equivalently, an orbiting transition state (OTS) model. This PSL model is appropriate for ion–molecule complexes because the TS for the reverse, barrierless association process is accurately described as lying at the top of the centrifugal barrier. The 2-D external rotations are treated adiabatically (i.e., they are inactive) but with centrifugal effects included, consistent with the discussion of Waage and Rabinovitch.[29] The adiabatic 2-D rotational energy of the EM is assumed to have a statistical distribution with explicit summation over the possible values of the rotational quantum number.[3] The normalized distribution of the angular momentum quantum number is given by Eq. (8):

$$f(J)=(2J+1)\rho[E^*-E_R(J)]\Big/\sum_{J=0}^{J_{max}}[(2J+1)\rho(E^*-E_R(J)]. \quad (8)$$

For each J, the rotational energy of the complex is given as $E_R(J)=hcBJ(J+1)$. We also note that $E_R^\dagger(J)$ is restricted to values less than or equal to $E_R(J)$. This restriction simply reflects the fact that the rotational constant (moment of inertia) of the TS, $B^\dagger$ ($I^\dagger$) should never be greater (less) than that

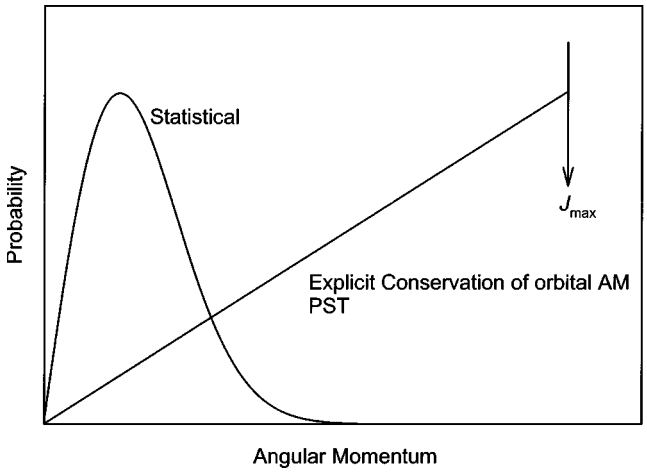

FIG. 3. Distributions of the angular momentum quantum number J of the inactive 2-D rotor of energized molecules appropriate for model 1 (statistical), model 2 (explicit conservation of orbital angular momentum), and phase space theory (PST), where the latter two are identical.

for the EM, B (I), because this would mean that the separation of products at the centrifugal barrier is smaller than it is in the EM, which is physically unrealistic.

The angular momentum distribution of Eq. (8) is shown in Fig. 3. The distribution is concentrated at low values of J because only a small amount of the available energy, E^*, is partitioned into the 2-D rotational modes for a modest-sized or larger EM.

2. Explicit conservation of orbital angular momentum ($J=L$)

The statistical distribution of Eq. (8) is unrealistic for a reaction that involves complex formation because the majority of reactant collisions occur with nonzero impact parameters, b_0 (where we will use the zero subscript to designate properties of reactants). Unlike the CID process where the third-body (Rg) can carry away most of the angular momentum from the complex, collisions with nonzero impact parameters produce rapidly rotating complexes because of angular momentum conservation. This is demonstrated by remembering that the orbital angular momentum vector (designated by bold characters) is given by the relation $\mathbf{L}_0 = \mu_0 v_0 b_0$, where v_0 is the relative velocity and μ_0 is the reduced mass of the reactants. For an association reaction, the conservation of angular momentum requires that the rotational angular momentum of the complex be given by $\mathbf{L}_0$ if the rotational angular momentum of the reactants is ignored. This is a reasonable approximation, as discussed in Appendix B.[18]

In order to construct a model that conserves orbital angular momentum explicitly, we start with the definition of the collision cross section, Eq. (9):

$$\sigma(E) = \int_0^{b_{max}} 2\pi b_0 \, db_0 . \tag{9}$$

Here, the critical impact parameter b_{max} for the LGS collision capture model, Eq. (4), is given by $b_{max} = (2\alpha e^2/4\pi\varepsilon_0 E)^{1/4}$. If the long-range potential includes an ion–dipole term, the needed equations are given in Appendix A.[40] The impact parameter can be related to the angular momentum quantum number for rotation of the complex using the relation $\mathbf{L}_0 = \mu_0 v_0 b_0 = [J(J+1)\hbar^2]^{1/2}$. From these relations, substituting for b_0 in Eq. (9) yields the collision cross section in terms of the rotational quantum number of the EM,

$$\sigma(E) = \frac{\pi\hbar^2}{2E\mu} \int_0^{J_{max}} (2J+1) dJ, \tag{10}$$

where J_{max} is defined in Eq. (11):

$$J_{max}(J_{max}+1) = (2\mu^2\alpha e^2 E/\pi\varepsilon_0\hbar^4)^{1/2}. \tag{11}$$

The integration in Eq. (10) gives $\sigma(E) = (\pi\hbar^2/2E\mu) J_{max}(J_{max}+1) = \pi(2\alpha e^2/4\pi\varepsilon_0 E)^{1/2} = \sigma_{LGS}$.

To obtain the cross section for the formation of the association complex, we now introduce the summation over reactant internal energy and the exponential lifetime probability into Eq. (10) to obtain

$$\sigma_{ass}(E) = \frac{\pi\hbar^2}{2E\mu} \sum_i g_i \int_0^{J_{max}} (2J+1) \times \exp[-k_{Tot}(E^*,J)\tau] dJ. \tag{12}$$

A comparison of Eqs. (6) and (12) indicates that $f(J) = (2J+1)/J_{max}(J_{max}+1)$ for model 2, such that the only difference between models 1 and 2 is the distribution of the angular momentum of the EM. A comparison of those distributions shows a significant difference (Fig. 3). Unlike the model 1 distribution, which has a concentration at low values of J, the model 2 distribution is a linearly increasing function up to J_{max}. This is the precise angular momentum distribution of the EM if the reactant orbital angular momentum does not couple with reactant rotational angular momentum.

For a PSL transition state defined by the centrifugal barrier, the separation of ion–neutral fragments is given by Eq. (13). Equation (14) gives the barrier height as a function of the orbital angular momentum of the products, L:[3]

$$r^* = [\alpha e^2\mu/2\pi\varepsilon_0 L(L+1)\hbar^2]^{1/2}, \tag{13}$$

$$V_{eff}(r^*) = \pi\varepsilon_0\hbar^4 L^2(L+1)^2/2\alpha e^2\mu^2. \tag{14}$$

From Fig. 4, it is easy to see that the minimum energy required for the EM to reach the TS is $E_0 + V_{eff}(r^*)$. Because the potential barrier is a quartic function of L and L is set equal to J in models 1 and 2, complexes having large J have a very long lifetime. Note that complexes with large J are unlikely for model 1, as seen in Fig. 3.

The energy-dependent rate constant for model 2 for the $Na^+ + DXE$ reaction, averaged over a proper J distribution, is compared with the rate constant for model 1 in Fig. 5. Despite the major difference in the distribution of the angular momentum for the inactive 2-D rotor of the EMs, the rate constants averaged over J distributions are of the same order of magnitude. To see why this is reasonable, consider the rate constant as a function of total angular momentum J. The rate constant becomes larger when J increases up to some J, the centrifugal acceleration discussed by Waage and Rabinovitch.[29] However, the rate constant is not a monotonically increasing function of J because the rate constant must

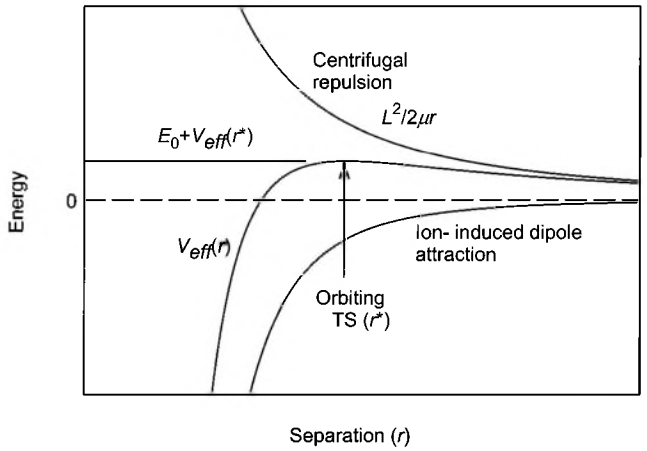

FIG. 4. The potential energy surface for an orbiting transition state. The effective potential, $V_{\text{eff}}(r)$, is given by the sum of the attractive potential (i.e., ion-induced dipole potential) and the centrifugal repulsion. $V_{\text{eff}}(r)$ reaches a maximum at r^*, the separation of two productlike fragments at the transition state. The minimum energy required for the complex to dissociate is given by E_0, the bond dissociation energy, plus the centrifugal barrier height, $V_{\text{eff}}(r^*)$.

go to zero as a J approaches $J_{\max}$. In addition, we note that the number of states at the TS, $N^{\dagger}[E^*-E_R^{\dagger}(J)-E_0]$, is heavily weighted toward small values of $E_R^{\dagger}(J)$ by the density of vibrational states. In essence, this latter factor introduces an intrinsic statistical weighting to the calculation of the rate constant in model 2.

3. Phase space theory

In the phase space theory (PST) approach, the coupling between orbital angular momentum and rotational angular momentum is allowed in such a way that total angular momentum is conserved explicitly. Throughout this section, we work with classical PST, i.e., $J(J+1)\rightarrow J^2$ and $(2J+1)\rightarrow 2J$, because it is considerably faster than the quantum form while giving essentially identical results.[17] The common assumption[18] that total angular momentum of the EM is

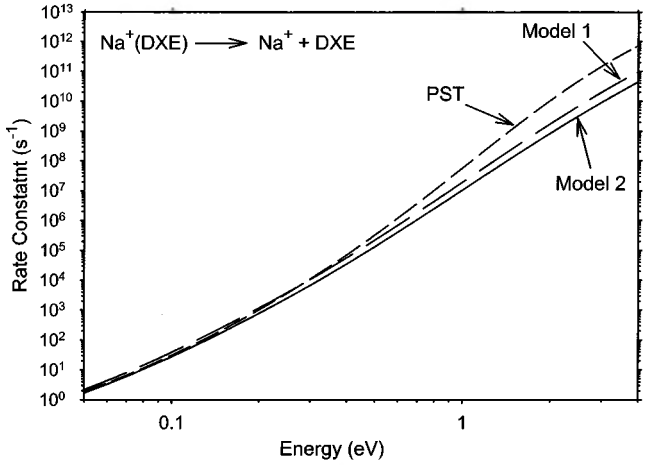

FIG. 5. Rate constants for the $Na^+ + DXE$ reaction for model 1 (long dashed), model 2 (solid line), and phase space theory (short dashed) as a function of energy. All rate constants are calculated using a bond dissociation energy of 1.78 eV and are integrated over the appropriate angular momentum distribution.

entirely generated by orbital angular momentum is used throughout this section. (Appendix B explores the more rigorous treatment where the orbital and rotational angular momenta of the reactants are allowed to couple to yield the angular momentum in the EM.) Given this assumption, the cross section for association is calculated using Eq. (12), where PST differs from model 2 in the calculation of the rate constant, $k(E^*,J)$. For the explicit calculation of rates, we adopt the approach used by Bowers and co-workers.[17,18] The following details the differences between this PST approach to calculating $k(E^*,J)$ and that discussed above for Eq. (7).

The sum of states for any molecule is calculated by the following procedure. As noted above, the energy available to the EM is $E^*=E+E_i+E_0$. We assume that vibrational and rotational motions are separable such that one can partition the energy of the orbiting transition state (OTS) as

$$E+E_i=E_V+E_R^{\dagger}(L)+E_r^{\dagger}(J_r)=E_V+E_{\text{TotR}}^{\dagger}, \tag{15}$$

where E_V, $E_R^{\dagger}(L)$, $E_r^{\dagger}(J_r)$, $E_{\text{TotR}}^{\dagger}$ are the vibrational energy, the 2-D external rotational energy that depends on the orbital angular momentum quantum number L, the rotational energy of the products that depends on the rotational angular momentum quantum number J_r (here, the lower case r stands for fragment rotation), and the total rotational energy, respectively. Then the sum of states for the OTS at a total angular momentum designated by the quantum number J is given as

$$N^{\dagger}(E^*-E_{\text{TotR}}^{\dagger}-E_0,J) = \int_0^{E^*-E_0} \rho_v(E^*-E_{\text{TotR}}^{\dagger}-E_0)\Gamma(E_{\text{TotR}}^{\dagger},J)dE_{\text{TotR}}^{\dagger}, \tag{16}$$

where $\rho_v(E^*-E_{\text{TotR}}^{\dagger}-E_0)$ and $\Gamma(E_{\text{TotR}}^{\dagger},J)$ are the vibrational density of states and the total rotational sum of states of the products, respectively. The total rotational sum of states of the OTS at $E_{\text{TotR}}^{\dagger}$ and J is given by Eq. (17),

$$\Gamma(E_{\text{TotR}}^{\dagger},J)=\int\int \theta(J_r,L)\Gamma(E_r^{\dagger},J_r)dJ_r\,dL, \tag{17}$$

where $\Gamma(E_r^{\dagger},J_r)$ is the rotational sum of states, and $\theta(J_r,L)$ is unity within the boundary shown in Fig. 6 and zero outside.[18] The boundaries are given by angular momentum conservation ($J=L+J_r, J=L-J_r, J=J_r-L$) and the total rotational energy curve is given by Eq. (18),

$$E_{\text{TotR}}^{\dagger}=\pi\varepsilon_0\hbar^4L^4/2\alpha e^2\mu^2+hcBJ^2, \tag{18}$$

where the first and second terms can be recognized as classical expressions for the effective potential barrier height, Eq. (14), and the rotational energy. The rotational sum of states for an atom spheroid (i.e., the situation of interest here in which the product fragments are a bare atomic ion and a neutral that is treated as a sphere) is given as $2J_r$. (For other types of systems, the appropriate equations are given elsewhere.[17]) Note that we use the approximation that the DXE neutral is represented as a spherical top molecule. The description of DXE as a prolate rotor was also investigated, as described in detail elsewhere.[41] The error associated with this approximation is small, as indicated by Chesnavich and Bowers.[17]

For PST, the density of states is calculated by Eq. (19),

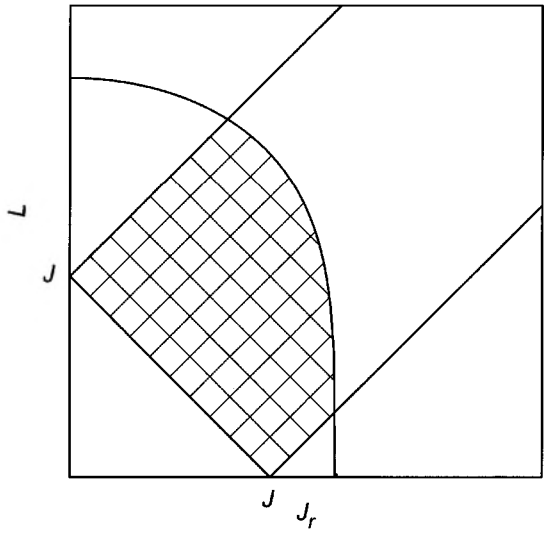

FIG. 6. A diagram showing the conservation of angular momentum in phase space theory. The straight lines indicate the values of $L+J_r$, $|L-J_r|$, and $|J_r-L|$. The curved line is defined by energy conservation and is specified in Eq. (18). The values of L and J_r for which angular momentum can be conserved (the ϑ function referred to in the text) is indicated by the hatched region.

$$\rho(E)=2J\rho_v[E^*-E_{\text{R3-D}}(J)], \tag{19}$$

where $\rho_v[E^*-E_{\text{R3-D}}(J)]$ and $E_{\text{R3-D}}(J)$ are the vibrational density of states and the rotational energy of the energized molecule, where the 3-D designation indicates that all three rotational modes are included, respectively. The $2J$ term accounts for the degeneracy of the spherical rotor. (For a linear EM, this term is equal to unity.)

Thus, the PST rate constant is given by

$$k(E^*,J)=sN^\dagger(E^*-E^\dagger_{\text{Tot}R}-E_0,J)/h2J\rho_v[E^*-E_{\text{R3-D}}(J)], \tag{20}$$

where the only difference between Eq. (7) and Eq. (20) is the treatment of rotational energies. In Eq. (7), the external 2-D rotations are treated as inactive modes, whereas in the PST expression, the 2-D external rotations are treated as active modes as long as total angular momentum is conserved. In PST, the rotations of the productlike fragments at the OTS are also restricted by the conservation of total angular momentum, whereas in models 1 and 2, these rotations are restricted only by energy conservation

The energy-dependent rate constant, averaged over the proper J distribution, for PST is larger at higher energies than those for models 2 for Na^+ and K^+ with the DXE reaction, as shown for the Na^+ system in Fig. 5. The increase in the PST rate constant is a direct consequence of the coupling of the orbital and rotational angular momentum. Because the majority of the EMs formed by association have high angular momenta (Fig. 3), the centrifugal barrier at the OTS for dissociation is necessarily high for model 2, in which the orbital angular momentum quantum number L is equal to J. As a consequence, the complex is long-lived. However, in the PST approach, the centrifugal barrier can be lower because the orbital angular momentum can couple with rotational angular momentum of the products. The larger the angular momentum (which increases with kinetic energy), the larger the effect is. Because the vibrational density of states in Eq. (16) is a maximum for small values of $E^\dagger_{\text{Tot}R}$ and declines rapidly with increasing $E^\dagger_{\text{Tot}R}$, small values of $E^\dagger_{\text{Tot}R}$ are statistically favored, such that small centrifugal barriers dominate the decomposition pathways. This statistical preference also helps explain why the PST rate constants (and as noted above, for model 2 as well) do not differ drastically from model 1, where the rotational energies are simply assumed to be statistical. We also note that at low energies the rates from model 1 are slightly larger than those from PST, a consequence of the failure to conserve angular momentum.

The enhancement in the PST rate constants for the Li^+ +DXE reaction (not shown) compared to model 2 is much smaller than in the Na^+ and K^+ systems at all energies. This is partly a consequence of the deeper potential well, E_0, which reduces the effect of removing rotational energy from the energy available to the TS and EM. It is also related to the magnitude of the value of $J_{\max}$, which is smaller for a smaller reduced mass, Eq. (11). This reduces the area of the accessible phase space allowed by angular momentum conservation (the hatched area in Fig. 6), thereby reducing the effect of lowering the centrifugal barrier by coupling with product rotation.

C. Analysis of the experimental cross sections

Experimental cross sections for the associative reactions are reproduced with the different models described above, as shown in Fig. 7. It is important to realize that the only adjustable parameter in all three models is E_0, the bond energy of M^+–DXE. This controls the absolute magnitude and shape of the predicted cross sections. The vibrational frequencies and rotational constants of the DXE reactant and M^+(DXE) complexes are calculated at the B3LYP/6-31 +G* level of theory and frequencies are scaled by 0.9613.[42] Because our absolute cross sections are reported to have ±20% uncertainties in magnitude, estimates of the uncertainties in the threshold energies are obtained by fitting to the experimental cross sections scaled by ±20%, and also include variations in the time available for reaction by factors of 2 and 1/2, variations associated with uncertainties in the vibrational frequencies by ±10%, and the error in the absolute energy scale (±0.05 eV lab). The results for all models are listed in Table I along with BDEs from our experimental CID study and theory (MP2/6-31+G* level).[7–9]

1. Statistically distributed inactive 2-D rotor

This model reproduces all three experimental cross sections both in magnitude and shape. For the Li^++DXE association reaction, the best fit to the experimental cross section yields an E_0 of 2.45±0.19 eV, in very good agreement with our previous CID (2.50±0.19 eV) and theoretical results (2.65 eV).[7] Clearly, this model cross section does not fit the experimental cross sections at very low energies (and as will be seen, none of the models do any better). As noted above, we believe that the experimental cross section is low in this case because some complexes are backscattered in the laboratory frame and not detected, a consequence of the nonnegligible thermal motion of the DXE at low energy and the light mass of the Li^+ ion. The model also deviates from the

experimental cross section at very high energies. (Again, all of the models underestimate the experimental cross sections at high energies.) The deviation at higher energies may be caused by a collisional relaxation with the residual gases in our apparatus. Collisions with such background gases would yield association complexes no matter what the DXE pressure, leaving a finite cross section even upon extrapolation of the DXE pressure to zero. The $Li^+(DXE)$ system is most sensitive to this effect because this complex has the longest lifetime among the systems studied here.

For the $Na^+ + DXE$ and $K^+ + DXE$ reactions, the best fits of the experimental cross sections yield BDEs of 1.78 ± 0.13 and 1.28 ± 0.11 eV, respectively. Again, the BDEs for $Na^+ + DXE$ and $K^+ + DXE$ are in good agreement with our previous CID (1.64 ± 0.04 and 1.23 ± 0.04 eV, respectively) and theoretical results (1.79 and 1.39 eV, respectively).[8,9] Note that the model reproduces both experimental cross sections nicely at low energies, consistent with negligible backscattering for the heavier ions.

2. Explicit conservation of orbital angular momentum

For the $Li^+ + DXE$ experiment, the best fit to the experimental data yields $E_0 = 2.40 \pm 0.18$ eV, in excellent agreement with our previous CID results and theory. Again the model is too large at very low energies and too small at high energies for the reasons described above.

In the $Na^+ + DXE$ experiment, the best fit to the experimental cross sections yields $E_0 = 1.75 \pm 0.13$ eV, in good agreement with our previous CID results and theory.[8] For this reaction, the model cross section fits the experimental cross section well for most energies but exhibits a tail at very high energies. The tail is caused by trajectories with large angular momenta, where they tend to stay as a complex for a long time because of the high centrifugal barrier (proportional to L^4). Such a tail is absent in the $Li^+ + DXE$ reaction, which can be understood as follows: The $Li^+(DXE)$ association complex has a small maximum angular momentum quantum number (J_{max}) compared to the $Na^+(DXE)$ and $K^+(DXE)$ association complexes because of the smaller reduced mass in the $Li^+ + DXE$ reaction, Eq. (11). However, the 2-D rotational constant of the EM, B, changes by only 10% between the $Na^+(DXE)$ and $Li^+(DXE)$ complexes, such that the maximum value of $E_R(J)$ is much smaller in the $Li^+ + DXE$ reaction for the same impact parameter and relative energy. Because $E_R^\dagger(J)$ is restricted to values less than or equal to $E_R(J)$, the dissociation rate constant calculated in Eq. (7) increases for the $Li^+ + DXE$ reaction for angular momenta approaching J_{max}. This enhanced rate constant eliminates the long-lived complexes associated with large J values, hence, no tail is observed in the $Li^+ + DXE$ reaction.

For the $K^+ + DXE$ experiment, the best fit to the experimental cross section for this reaction yields $E_0 = 1.28 \pm 0.10$ eV, which nearly coincides with our previous CID results and theory.[9] As in the Na^+ case, the best fit using model 2 predicts the cross section magnitude and the energy dependence of the experimental cross section. No tail is observed in the $K^+ + DXE$ reaction but only because the $K^+(DXE)$ association cross section is small.

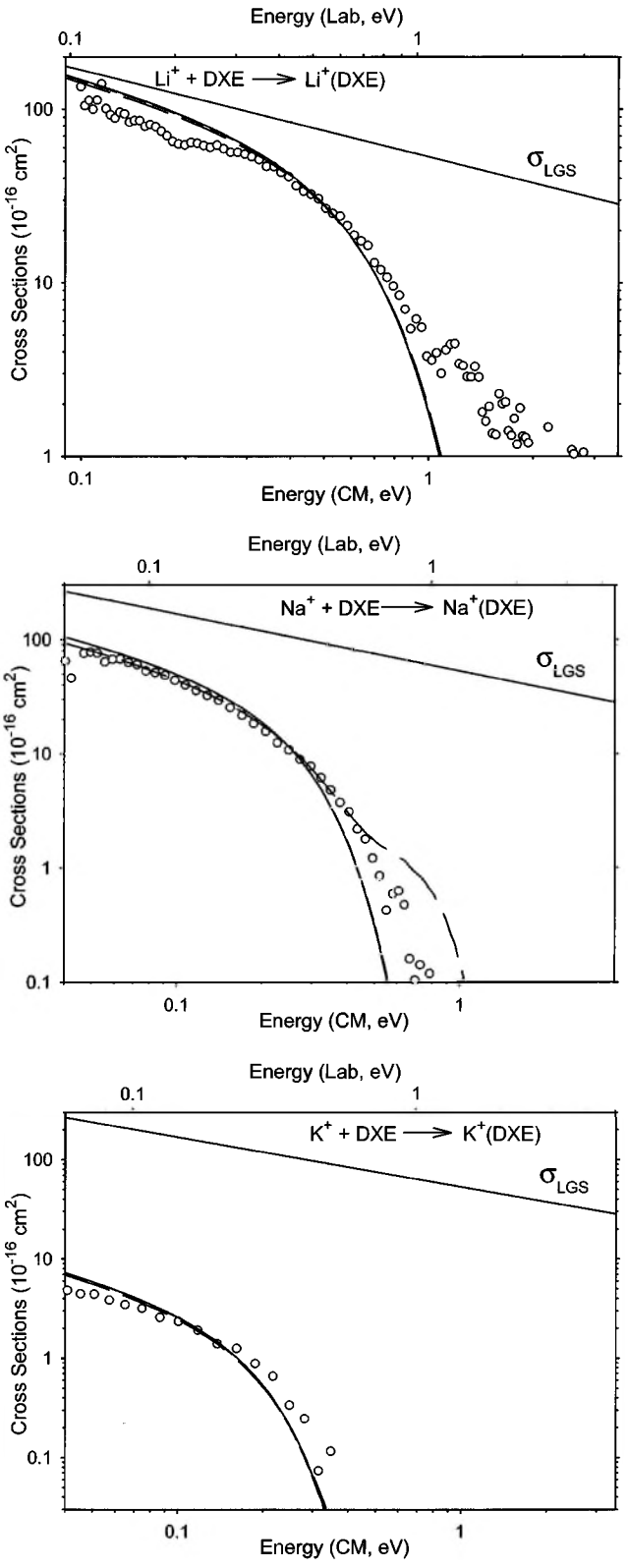

FIG. 7. Comparisons of the experimental data with models for the association reactions of alkali metal ions (Li^+,Na^+,K^+) with DXE as a function of kinetic energy in the center-of-mass frame (lower x axis) and laboratory frame (upper x axis). Open circles show zero pressure extrapolated cross sections. Results for the statistical model (model 1, short dashed), explicit conservation of orbital angular momentum (model 2, long dashed), and phase space theory (solid line) calculated using the bond energies listed in Table I are shown. The LGS cross section, Eq. (4), is also indicated.

TABLE I. Bond dissociation energies (eV).

Reaction	Theory	CID	Association		
			Statistical	Orb. AM cons.	PST
$Li^+ + DXE$	2.65	2.50±0.19	2.45±0.19	2.40±0.18	2.46±0.19
$Na^+ + DXE$	1.79	1.64±0.04	1.78±0.13	1.75±0.13	1.78±0.13
$K^+ + DXE$	1.39	1.23±0.04	1.28±0.11	1.28±0.10	1.29±0.10
MAD[a] (theory)		0.15±0.01	0.11±0.10	0.13±0.11	0.10±0.09
MAD[a] (CID)	0.15±0.01		0.08±0.05	0.09±0.03	0.08±0.05

[a]Mean absolute deviation.

3. Phase space theory

The best fits to the three association cross sections when using PST are obtained when E_0 is set to 2.46±0.19, 1.78 ±0.13, and 1.29±0.10 eV for the Li^+, Na^+, and K^+ +DXE experiments, respectively. These results are in excellent agreement with both CID results and theory[7–9] and nearly identical with the other models. The PST model cross sections are nearly identical to the model 1 cross section in both shape and magnitude for all cases studied here. As with the other models, the model at very low energies and high energy for the $Li^+ + DXE$ experiment deviates from the experimental cross section because of the reasons described above. Note that the high-energy tail observed in model 2, a consequence of having a large centrifugal barrier, is absent in all three PST models. As discussed above, this is because PST allows such rapidly rotating energized molecules to dissociate by lowering the centrifugal barrier.

4. Effect of dipole moment

As noted above, the lowest-energy conformer of DXE (*trans, trans, trans*; *ttt*) has no permanent dipole moment, but the next highest-energy conformer (*trans, gauche, trans*; *tgt*), which lies only 0.4–0.8 kJ/mol higher in energy,[7] does (estimated to be 2.0 D). Therefore, it is possible that the experimental association reactions are influenced by interactions with the *tgt* conformer. Using formulas outlined elsewhere[40] and in Appendix A, the effect of a locked dipole on the reactions can be included in the modeling performed here. This will overestimate the experimental effect both because the locked dipole overestimates the collision cross section for a rotating molecule and because the population of the *tgt* conformer is less than half of the available reactant population. We find (using either model 2 or PST) that including the dipole decreases the optimum bond energies needed to reproduce the data by 0.3, 0.04, and 0.01 eV for the Li^+, Na^+, and K^+ systems, respectively. Further, the predicted association cross sections fall off more rapidly than those without the dipole included, such that they do not reproduce the experimental cross sections at higher energies as well as those shown in Fig. 7. For model 2, we also incorporated an estimate of the effect of the dipole using cross sections estimated with Su's trajectory results,[43] which yields a more realistic collision cross section that lies between the LGS and locked dipole models. For the $Li^+(DXE)$ system, the trajectory calculations yield an optimum bond energy that lies 0.1 eV below the value in Table I. Overall, it is clear that any realistic effect of a dipole moment on the present results is well within the experimental errors cited with the values listed in Table I for all three metal systems.

IV. CONCLUSION

Association reactions of bare alkali metal ions (Li^+, Na^+, and K^+) and DXE are studied using kinetic energy-dependent mass spectrometry. In this paper, we assume that the lifetimes of the association complexes are limited by the passage over a loose, orbiting (PSL) transition state and analyze the experimental cross sections by using three models: the statistical distribution of orbital angular momentum, the explicit conservation of orbital angular momentum, and phase space theory. All methods involve careful treatments of lifetime effects, kinetic energy distributions of the ion and neutral reactants, reactant internal energy distributions, and angular momentum distributions. The resulting model cross sections reproduce the kinetic energy dependences and absolute magnitudes of our experimental cross sections in detail using only a single adjustable parameter, E_0. Compared with results from our previous CID experiments and theory,[7–9] all three models for the association cross sections reproduce the bond dissociation energies excellently, verifying that the analysis of association reactions (and its underlying assumptions) is a useful means of acquiring thermodynamic information.

In this regard, we believe that this methodology should be useful for much larger systems. In such cases, one anticipates that the lifetimes of the energized molecules will increase, such that the association cross section will saturate at the collision limit for low energies. If measurements at only thermal energies (such as in ICR experiments) are made, then such data can only be interpreted to provide a lower limit to the bond energy of interest. However, the guided ion beam instrument allows the energy of the complex to be increased extensively, until dissociation on the time scale of the experiment can be induced. Thus, by modeling the high-energy decline in the association cross section, thermodynamic data can still be obtained for such large, long-lived systems.

An important facet of the present work compared to the CID studies is that the bimolecular reaction of M^+ with DXE forms an energized $M^+(DXE)$ complex with a well-defined internal energy distribution and a broad but known angular momentum distribution. Because these carefully analyzed results of association reactions are in excellent agreement with

those obtained from an analysis of CID data on the same systems,[7–9] the present study verifies the accuracy of our assumptions regarding the use of statistical theory to describe kinetic shifts observed in CID studies.[3] Further, we observe that very different assumptions about the angular momentum distributions still allow accurate modeling of the association reactions with bond energies that are identical within experimental error. This indicates that the thermochemistry derived from modeling of association and probably CID processes is not particularly sensitive to such distributions.

ACKNOWLEDGMENTS

This work is supported by the National Science Foundation, Grant No. CHE-0135517. HK thanks Professor K. Ervin for helpful conversations and Professor R. Dunbar for help with the VARIFLEX code.

APPENDIX A: INCLUSION OF LOCKED DIPOLE

The effect of including a dipole term in the potential for an ion–molecule reaction has been examined previously[44] and many of the relevant equations for CID processes have been summarized by Iceman and Armentrout.[40] Here, the equations needed to include a locked-dipole potential for association reactions are summarized. The potential of the ion–locked-dipole interaction is given as

$$V_{\mathrm{eff}}(r)=J(J+1)\hbar^2/2\mu r^2-M_D e/4\pi\varepsilon_0 r^2 - \alpha e^2/8\pi\varepsilon_0 r^4, \tag{A1}$$

where M_D is the dipole moment of the neutral and all other quantities are defined in the text. By following the same approach used in Sec. III B, we obtain $J_{\max}^{\mathrm{LD}}$ as

$$J_{\max}^{\mathrm{LD}}(J_{\max}^{\mathrm{LD}}+1)=[(2\alpha e^2\mu^2 E/\pi\varepsilon_0)^{1/2} + M_D\mu^2 e/2\pi\varepsilon_0]/\hbar^2. \tag{A2}$$

Similarly, the separation of ion–neutral fragments at the centrifugal barrier is given by Eq. (A3) and Eq. (A4) provides the barrier height as a function of the orbital angular momentum quantum number J:

$$r^*=\alpha e^2/[2\pi\varepsilon_0 J(J+1)\hbar^2/\mu-(M_D e)], \tag{A3}$$

$$V_{\mathrm{eff}}(r^*)=\pi\varepsilon_0[J(J+1)\hbar^2/\mu-(M_D e/2\pi\varepsilon_0)]^2/2\alpha e^2. \tag{A4}$$

Finally, the rotational constant of the OTS for the ion–locked dipole potential is given as

$$B^{\dagger}=\varepsilon_0 h[J(J+1)\hbar^2/\mu-M_D e/2\pi\varepsilon_0]/4\pi c\mu^2 e^2\alpha. \tag{A5}$$

The total collision cross section that includes the ion–locked dipole interaction is given by Eq. (A6):

$$\sigma_{\mathrm{LD}}(E)=\sigma_{\mathrm{LGS}}(E)+e\mu_D/4\varepsilon_0 E. \tag{A6}$$

APPENDIX B: REACTANT ROTATIONAL COUPLING

The classical probability of forming an energized molecule (EM) with a total angular momentum (J) for a given orbital angular momentum (L_0) and rotational angular momentum (J_{r0}) of reactants is given as Eq. (B1):

$$f(J|J_{r0},L_0)=\begin{cases}0, & J<|L_0-J_{r0}|,\\ 2J/2J_{r0}2L_0, & |L_0-J_{r0}|\leq J\leq L_0+J_{r0},\\ 0, & L_0+J_{r0}<J.\end{cases} \tag{B1}$$

We treat the rotational angular momentum distribution of the reactants as given by a Maxwell–Boltzmann distribution and the orbital angular momentum is determined by the impact parameter distribution. Thus, the probability distribution of J for a given J_{r0} and L_0 is given by Eq. (B2),

$$P(J)dJ=\int\int f(J|J_{r0},L_0)Q(J_{r0})2J_0/L_{0\,\max}^2\,dJ_{r0}\,dL_0, \tag{B2}$$

where $Q(J_{r0})$ is the Maxwell–Boltzmann distribution for a spherical reactant. This distribution is given in Eq. (B3),

$$Q(J_{r0})dJ_{r0}=2J_{r0}^2\exp[-hcBJ_{r0}^2/kT]1\Big/\int_0^{J_{r0}^*}2J_{r0}^2\exp[-hcBJ_{r0}^2/kT]dJ_{r0}, \tag{B3}$$

where J_{r0}^* is bounded by the internal energy of the reactant. Note that the summation in Eq. (B2) is restricted by angular momentum conservation, Eq. (B1). The average rate constant is given in Eq. (B4):

$$k(E)=\int k(E,J)P(J)dJ. \tag{B4}$$

The association cross section, σ_{ass}, and product cross sections, σ_x, are given by Eqs. (B5) and (B6), respectively,

$$\sigma_{\mathrm{ass}}(E)=\frac{\pi\hbar^2}{2E\mu}\sum_i g_i\int_0^{J_{r0}^*}Q(J_{r0})\times\int_0^{L_{0\,\max}}2L_0\int_0^{L_0+J_{r0}}f(J|L_0,J_{r0})\times\exp[-k_{\mathrm{tot}}(E+E_0+E_i,J)\tau]dJ\,dL_0\,dJ_{r0}, \tag{B5}$$

$$\sigma_x(E)=\frac{\pi\hbar^2}{2E\mu}\sum_i g_i\int_0^{J_{r0}^*}Q(J_{r0})\int_0^{L_{0\,\max}}2L_0\times\int_0^{L_0+J_{r0}}f(J|L_0,J_{r0})\frac{k_x(E+E_0+E_i-E_{0x},J)}{k_{\mathrm{tot}}(E+E_0+E_i,J)}\times\{1-\exp[-k_{\mathrm{tot}}(E+E_0+E_i,J)\tau]\}dJ\,dL_0\,dJ_{r0}, \tag{B6}$$

where $k_{\mathrm{tot}}(E+E_0+E_i,J)$ is given by

$$k_{\mathrm{tot}}(E+E_0+E_i,J)=\sum_x k_x(E+E_0+E_i-E_{0x},J). \tag{B7}$$

After integrating over L_0, Eqs. (B5) and (B6) become Eqs. (B8), and (B9), respectively,

$$\sigma_{ass}(E)=\frac{\pi\hbar^2}{2E\mu}\sum_i g_i\int_0^{J_{r0}^*}Q(J_{r0})\int_{L^-}^{L^+}\frac{2J}{2J_{r0}}\times(\min\{L_{0\,max},J+J_{r0}\}-|J-J_{r0}|)\times\exp[-k_{tot}(E+E_0+E_t,J)\tau]dJ\,dJ_{r0}, \quad (B8)$$

$$\sigma_x(E)=\frac{\pi\hbar^2}{2E\mu}\sum_i g_i\int_0^{J_{r0}^*}Q(J_{r0})\int_{L^-}^{L^+}\frac{2J}{2J_{r0}}\times(\min\{L_{0\,max},J+J_{r0}\}-|J-J_{r0}|)\times\frac{k_x(E+E_0+E_i-E_{0x},J)}{k_{tot}(E+E_0+E_i,J)}\times\exp[-k_{tot}(E+E_0+E_i,J)\tau]dJ\,dJ_{r0}, \quad (B9)$$

where L^+ and L^- are given as

$$L^+=\min\{L_{0\,max}+J_{r0},J_{max}^{OTS}(prod)\}, \quad (B10)$$

$$L^-=\max\{J_{r0}-L_{0\,max},0\}, \quad (B11)$$

where $J_{max}^{OTS}(prod)$ is defined as the maximum angular momentum, such that the sum of states becomes zero for any J larger than $J_{max}^{OTS}(prod)$.[21] Finally, we recover Eq. (12) by simply making the approximation that the rotational angular momentum is small, as expected. The differences in cross sections calculated with and without reactant rotational orbital coupling are small in all cases studied here.

[1] R. C. Dunbar, Int. J. Mass Spectrom. Ion Processes **160**, 1 (1997).
[2] S. J. Klippenstein, Y. Yang, V. Ryzhov, and R. C. Dunbar, J. Chem. Phys. **104**, 4502 (1996).
[3] M. T. Rodgers, K. M. Ervin, and P. B. Armentrout, J. Chem. Phys. **106**, 4499 (1997).
[4] M. T. Rodgers and P. B. Armentrout, J. Chem. Phys. **109**, 1787 (1998).
[5] M. T. Rodgers and P. B. Armentrout, J. Phys. Chem. **101**, 2614 (1997).
[6] M. B. More, E. D. Glendening, D. Ray, D. Feller, and P. B. Armentrout, J. Phys. Chem. **100**, 1605 (1996).
[7] D. Ray, D. Feller, M. B. More, E. D. Glendening, and P. B. Armentrout, J. Phys. Chem. **100**, 16117 (1996).
[8] M. B. More, D. Ray, and P. B. Armentrout, J. Phys. Chem. A **101**, 831 (1997).
[9] M. B. More, D. Ray, and P. B. Armentrout, J. Phys. Chem. A **101**, 4254 (1997).
[10] M. B. More, D. Ray, and P. B. Armentrout, J. Phys. Chem. A **101**, 7007 (1997).
[11] M. B. More, D. Ray, and P. B. Armentrout, J. Am. Chem. Soc. **121**, 417 (1999).
[12] H. Koizumi, X.-G. Zhang, and P. B. Armentrout, J. Phys. Chem. A **105**, 2444 (2001).
[13] H. Koizumi and P. B. Armentrout, J. Am. Soc. Mass Spectrom. **12**, 480 (2001).
[14] R. A. Marcus and O. K. Rice, J. Phys. Colloid Chem. **55**, 894 (1951); R. A. Marcus, J. Chem. Phys. **20**, 359 (1952); H. M. Rosenstock, M. B. Wallenstein, A. L. Wahrhaftig, and H. Eyring, Proc. Natl. Acad. Sci. U.S.A. **38**, 667 (1952).
[15] P. Pechukas and J. C. Light, J. Chem. Phys. **42**, 3281 (1965); J. Lin and J. C. Light, *ibid.* **43**, 3209 (1965); J. C. Light, Discuss. Faraday Soc. **44**, 14 (1967).
[16] E. Nikitin, Teor. Eksp. Khim. **135**, 144, 428 (1965).
[17] W. J. Chesnavich and M. T. Bowers, J. Chem. Phys. **66**, 2306 (1977).
[18] W. J. Chesnavich and M. T. Bowers, J. Am. Chem. Soc. **98**, 8301 (1976).
[19] C. E. Klots, J. Phys. Chem. **75**, 1526 (1971).
[20] C. E. Klots, Z. Naturforsch. A **27A**, 553 (1972).
[21] D. A. Webb and W. J. Chesnavich, J. Phys. Chem. **87**, 3791 (1983).
[22] K. M. Ervin and P. B. Armentrout, J. Chem. Phys. **83**, 166 (1985).
[23] R. H. Schultz and P. B. Armentrout, Int. J. Mass Spectrom. Ion Processes **107**, 29 (1991).
[24] F. Muntean and P. B. Armentrout, J. Chem. Phys. **115**, 1213 (2001).
[25] R. H. Schultz, K. C. Crellin, and P. B. Armentrout, J. Am. Chem. Soc. **113**, 8590 (1991).
[26] D. Gerlich, in *State-Selected and State-to-State Ion–Molecule Reaction Dynamics, Part 1, Experiment*, Advances in Chemical Physics Series, edited by C. Y. Ng and M. Baer (Wiley, New York, 1992), Vol. LXXXII, p. 1.
[27] G. Gioumousis and D. P. Stevenson, J. Chem. Phys. **29**, 294 (1958).
[28] K. J. Miller, J. Am. Chem. Soc. **112**, 8533 (1990).
[29] E. V. Waage and B. S. Rabinovitch, Chem. Rev. **70**, 377 (1970).
[30] R. C. Dunbar, Spectrochim. Acta, Part A **31A**, 797 (1975).
[31] S. J. Klippenstein, A. F. Wagner, R. C. Dunbar, D. M. Wardlaw, and S. H. Robertson, VARIFLEX, Version 1.0, 1999.
[32] C. Lifshitz, R. L. C. Wu, T. O. Tiernan, and D. T. J. Terwilliger, Chem. Phys. **68**, 247 (1978).
[33] P. J. Chantry, J. Chem. Phys. **55**, 2746 (1971).
[34] V. F. Deturi and K. M. Ervin, J. Phys. Chem. **103**, 6911 (1999).
[35] T. S. Beyer and D. F. Swinehart, Comm. Assoc. Computing Machinery **16**, 379 (1973).
[36] S. E. Stein and B. S. Rabinovitch, J. Chem. Phys. **58**, 2438 (1973).
[37] S. E. Stein and B. S. Rabinovitch, Chem. Phys. Lett. **49**, 183 (1977).
[38] R. G. Gilbert and S. C. Smith, *Theory of Unimolecular and Recombination Reactions* (Blackwell Scientific Publications, Oxford, 1990).
[39] F. Muntean, L. Heumann, and P. B. Armentrout, J. Chem. Phys. **116**, 5593 (2002).
[40] C. Iceman and P. B. Armentrout, Int. J. Mass. Spectrom. **222**, 329 (2003).
[41] H. Koizumi, Ph.D. thesis, University of Utah, 2003.
[42] J. B. Foresman and A. E. Frisch, *Exploring Chemistry with Electronic Structure Methods*, 2nd ed. (Gaussian, Inc., Pittsburgh, PA, 1996).
[43] T. Su, J. Chem. Phys. **100**, 4703 (1994).
[44] T. Su and M. T. Bowers, in *Gas Phase Ion Chemistry*, edited by M. T. Bowers (Academic, New York, 1979), Vol. 1, p. 83.